Synthesis and Evaluation of Novel Magnetic Composites of $SrFe_{12}O_{19}/CuO/TiO_2$ Nanoparticles for Visible Light Photodegradation of Methylene Blue

Jyothi Priya K.[1]*, Ramya Kumari Ch.[1], Suneetha M.[1], Swapna D.[1,2], Supriya G.[1], Padma M.[1] and Paul Douglas S.[1*]
1. Department of Engineering Chemistry, AU College of Engineering, Andhra University, Visakhapatnam-530003, INDIA
2. Dadi Institute of Engineering and Technology, Anakapalli- 531002, INDIA
*Priya.konathala94@gmail.com; spdfchem@andhrauniversity.edu.in

Abstract

Novel magnetic composites of $SrFe_{12}O_{19}/CuO/TiO_2$ nanoparticles were synthesized using the sol-gel method at low temperatures. X-ray diffraction (XRD), Fourier-transform infrared spectroscopy (FTIR), Scanning electron microscopy with energy-dispersive X-ray spectroscopy (SEM-EDX), Transmission electron microscopy (TEM), UV-Visible diffuse reflectance spectroscopy (UV-DRS) and Vibrating sample magnetometry (VSM) were used to characterize the structure, morphology and properties of these nanoparticles. The XRD revealed typical peaks for the nanocomposites including the anatase phase of TiO_2 with an average particle diameter of 8 nm. SEM scans revealed spherical particles, while EDAX analysis verified the existence of the component elements (Fe, Ti, O, Sr and Cu) in the nanocomposites. UV-DRS studies showed that the synthesized nanocomposite had a band-gap energy of 2.318 eV. VSM investigated the magnetic characteristics of $SrFe_{12}O_{19}$, including saturation magnetization (MS).

The catalytic performance of the produced nanocomposite was assessed by examining its capacity to destroy methylene blue dye under both visible and UV light. The photocatalytic studies showed that the $SrFe_{12}O_{19}/CuO/TiO_2$ nanocomposites degraded methylene blue dye with 100% efficiency. Under both forms of irradiation, the $SrFe_{12}O_{19}$/ CuO/ TiO_2 sample with a molar ratio of 0.8:0.1:0.1 demonstrated good catalytic efficiency and rate constant. The antibacterial activity investigations were done against Gram-negative Escherichia coli, Klebsiella pneumonia, Gram-positive Staphylococcus aureus and Bacillus Subtilis bacteria utilizing nanocomposites. Overall, the novel nanocomposites displayed strong photocatalytic activity and better antibacterial activity.

Keywords: $SrFe_{12}O_{19}/CuO/TiO_2$ nanomagnetic composites, Visible-light Photodegradation, Methylene blue.

Introduction

Organic dyes are prevalent contaminants in wastewater from various industries including leather, textile, cosmetics, food and paper[9]. Furthermore, synthetic dyes have been utilized in agricultural studies, light-harvesting arrays, photoelectrochemical cells and hair colouring[2]. Most dyes have been identified as pollutants since they are non-biodegradable and pose a risk to humans[1]. Chemical and biological oxidation, adsorption, electrochemical and membrane separation are some of the novel approaches for eliminating colours[3]. Furthermore, they may cause secondary pollution by moving organic contaminants from the liquid to the solid phase, necessitating further treatment[6].

Photocatalysis has lately received significant interest for its potential to break down and remove refractory wastewater from textile colors and finishing effluents[13]. The most widely used photocatalyst has been titanium oxide (TiO_2) nanoparticles with an electronic bandgap of 3.3 eV. However, as a metal oxide with a broadband gap, TiO_2 has only been used under ultraviolet light[4]. To absorb visible light, the band gap should be narrowed. Incorporating a metal oxide with a direct band gap of 1.5 eV such as CuO can boost TiO_2's ability as a photocatalyst[14]. Cupric oxide (CuO) is a photocatalytic material that may effectively remove and degrade various pollutants[15]. This semiconductor material's narrow bandgap allows it to absorb photons from the visible range[10].

CuO and TiO_2 have several advantages when mixed. The co-existence of CuO and TiO_2 lowers charge carrier recombination and improves photocatalytic activities[17]. Photocatalysts have enhanced photo responsibility and photo charge coincidence rates, but they are incapable of rapid separation and efficient recycling. Ferrite can be used to recycle photocatalysts efficiently[8]. $SrFe_{12}O_{19}$ is a hard magnetic material with excellent magnetic characteristics, corrosion resistance, chemical stability, cheap cost, superior mechanical qualities, high microwave magnetic loss and high-frequency responsiveness[11]. As a result, strontium hexaferrite ($SrFe_{12}O_{19}$) was chosen in the current investigation due to its unique magnetic properties which may aid in degrading efficiency. In this study, we attempted to synthesize a ternary $SrFe_{12}O_{19}/CuO/TiO_2$ nanocomposite for photo-catalytically eliminating methylene blue dye from an aqueous solution.

Material and Methods

The chemicals required to construct the $SrFe_{12}O_{19}$/ CuO/TiO_2 nanocomposite and other relevant research were purchased with AR grade (99% purity) and utilized without additional purification. Deionized water was used to prepare all the solutions for the experiments.

Table 1
Chemicals used to synthesize $SrFe_{12}O_{19}/CuO/TiO_2$ nanocomposite

Chemical compound	Chemical composition	Make
Titanium tetrachloride	$TiCl_4$	Loba Chemie
Strontium nitrate	$Sr(NO_3)_2$	Qualigens
Ferric citrate	$C_6H_5Fe_2O_7.3H_2O$	Sisco
Citric acid	$C_6H_8O_7.H_2O$	Loba Chemie
Copper nitrate	$Cu(NO_3)_2$	Loba Chemie
Hydrochloric acid	HCl	Molychem
Ammonium hydroxide	NH_4OH	Rankem
Ethylene glycol	$C_6H_6O_2$	Sisco

The materials that are used to synthesize $SrFe_{12}O_{19}/CuO/TiO_2$ are listed in the table 1.

Synthesis of $SrFe_{12}O_{19}$: The sol-gel route is applied for the preparation of $SrFe_{12}O_{19}$ magnetic particles. Add 20 ml of distilled water to each of 8.46 g of strontium nitrate, 143.5 g of ferric citrate and 25.2 g of citric acid to dissolve and make standard solutions. First, combine strontium nitrate and ferric citrate solutions, then add citric acid solution. Add NH_4OH solution to adjust the pH of the solution. Pour in 20 mL of ethylene glycol. After stirring for an hour, the solution is heated at 80 °C until the contents become dry powder. It is then calcined at 500 °C for an hour, annealed at 500 °C for an hour and ground to a fine powder.

Synthesis of CuO: 30 g $Cu(NO_3)_2$ is dissolved in 20 mL of distilled water followed by 20 mL of ethylene glycol. The solution is stirred for an hour and set aside for one day to gel. The ingredients are then dried at 200 °C till they form powder. There are then calcined for an hour at 300 °C, annealed at 500 °C for an hour and ground to a fine powder.

Synthesis of TiO_2: In this process, 6.9 ml of $TiCl_4$ (11.94 g) is gently disseminated in a beaker containing 350 ml of distilled water. A white curdy precipitate, possibly related to the production of Ortho titanic acid was obtained and held under magnetic stirring for 30 to 60 minutes to allow complete hydrolysis. The resulting mixture is heated at 80 °C to 100 °C on an electrical hot plate. It avoids chloride ion interference in the photocatalytic study and the final powder was dried in an electric hot air oven at roughly 80 °C to evaporate any moisture. Finally, the powder was ground in a mortar and pestle and calcined for 2 hours at 400 °C[12].

$TiCl_4 + H_2O \rightarrow [Ti(OH)_4] + H_2O$
(ortho titanic acid)

$[Ti(OH)_4] \rightarrow TiO_2 + 2H_2O$

Synthesis of $SrFe_{12}O_{19}/CuO/TiO_2$ Nanocomposites: The ternary $SrFe_{12}O_{19}/CuO/TiO_2$ nanocomposite is synthesized by combining previously synthesized $SrFe_{12}O_{19}$, CuO and TiO_2 nanoparticles in a 0.8: 0.1: 0.1 ratio and thoroughly mixing using a mortar and pestle.

Instrumentation: The phase of $SrFe_{12}O_{19}/CuO/TiO_2$ nanoparticles was analyzed using an X-ray diffractometer (Bruker DX-5) with $\lambda = 1.54$ Å at room temperature across a wide range of $10^{\circ} \leq 2\theta \leq 80^{\circ}$ and a scanning speed of 2 min^{-1}. The shape of the nanoparticles was investigated using a field emission scanning electron microscopy (FESEM) apparatus (Zeiss Gemini 300, Carl Zeiss, Germany). FTIR spectroscopy (IR Prestige-21, 400-4000 cm^{-1}) is utilized to analyze the adsorbent's functional groups. Band gaps are determined using the Shimadzu 2600R with a 200-800 nm range and $BaSO_4$ as a reference.

Results and Discussion

XRD analysis: The crystalline phase and purity are investigated using XRD analysis. The XRD pattern of $SrFe_{12}O_{19}/CuO/TiO_2$ is shown in fig. 1. All the observed prominent diffraction peaks are highly defined and may be assigned to the anatase phase TiO_2 at 2θ = 24.16 °, 37.2 °, 48.8 °, 54.1 °, 55.2°, 61.4 ° (JCPDS card no: 21-1272)[16], CuO at 2θ= 27.36 °, 34.2 °, 49.4 °, 58.3 °, 62.5 °, 66.2 ° (JCPDS card no: 48-1548)[5] and $SrFe_{12}O_{19}$ at 2θ = 30.3 °, 32.2 °, 33.1 °, 35.5 °, 36.4 °, 38.7 °, 40.4 °, 40.9 °, 57.4 °, 63.3 ° and 73.4 ° (JCPDS card no:24-1207)[7] respectively[15-].

Debye-Scherrer's formula calculated the average crystallite size of the samples:

$$D = 0.9\lambda/\beta \cos\theta$$

where D is the average crystalline size, 0.9 is the grain form factor, λ is the X-ray wavelength, β is the FWHM of the diffraction peak and θ is the incident angle. The average calculated crystal size of the ternary $SrFe_{12}O_{19}/CuO/TiO_2$ nanocomposite was found to be 8.737 nm.

UV-Vis DRS Analysis: The ultraviolet-visible diffuse reflectance spectroscopy (DRS) absorption spectra of $SrFe_{12}O_{19}/CuO/TiO_2$ nanoparticles (Fig. 2) revealed an absorption edge at 480 nm. The optical characteristics of nanoparticles are determined by studying the absorption spectra.

Energy band gap = $E_g = h\nu = hc/\lambda$

The optical band gap of TiO_2 nanoparticles is calculated using the following equation:

$(\alpha h\nu)^n = A(h\nu - E_g)$

where α is the absorption coefficient, hν is the photon energy, A is a constant relative to the material and n is either 2 for a direct band gap material or ½ for an indirect band gap material. The optical band gap for the absorption peak is calculated by extrapolating the linear section of the $(h\nu)^n$ vs. h curve to zero. The predicted energy band gap of $SrFe_{12}O_{19}/CuO/TiO_2$ absorption spectra in UV is 2.318 eV (Fig. 3).

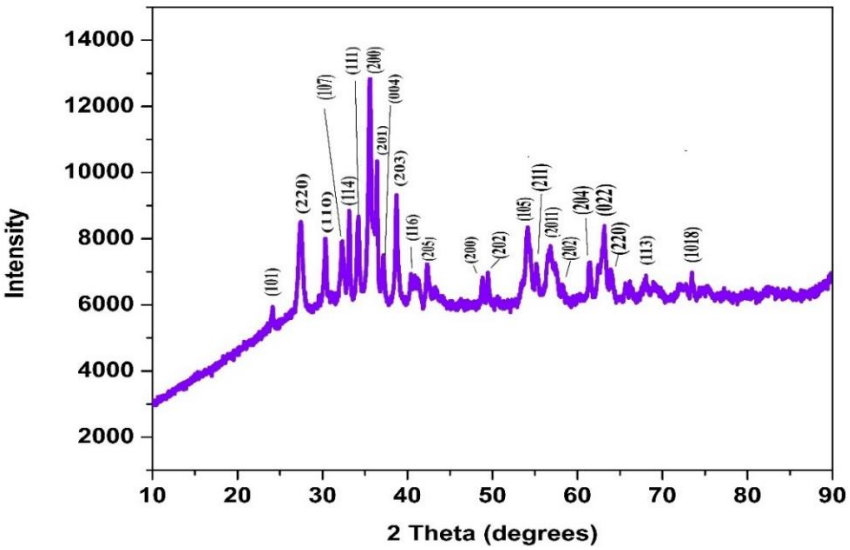

Fig. 1: XRD pattern of $SrFe_{12}O_{19}/CuO/TiO_2$

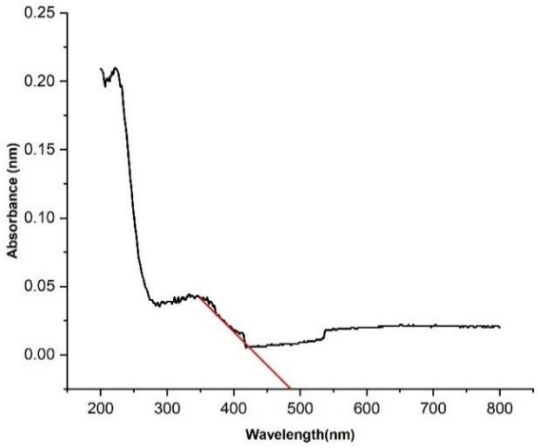

Fig. 2: UV-Visible absorption spectra of $SrFe_{12}O_{19}/CuO/TiO_2$

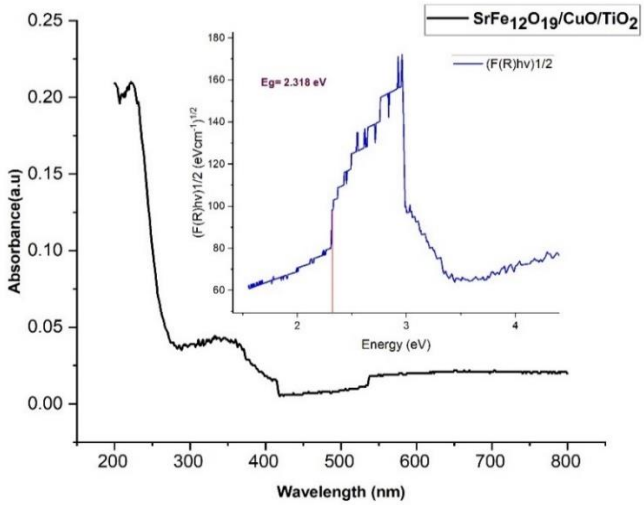

Fig. 3: Band gap of $SrFe_{12}O_{19}/CuO/TiO_2$

Scanning electron microscope and EDAX: The size and structure of nanoparticles determine their catalytic activity. Scanning electron microscopy is a high-resolution surface imaging technique. For surface imaging, the SEM employs an electron beam as a surface beam. Figure 4 exhibits the morphology of $SrFe_{12}O_{19}/CuO/TiO_2$ and clearly shows the existence of micro-structured particles produced in clusters as well as in certain needle-like features. It is clear that the treated sample contains nanoparticles with a diameter of 50 nm and an average particle size of 32.2 nm. An energy-dispersive X-ray spectroscopy (EDX) spectrum confirms the existence of Sr, Fe, Ti, Cu and O components (Fig. 5). These findings show that the materials were appropriately treated and so indirectly confirm the composite fabrication.

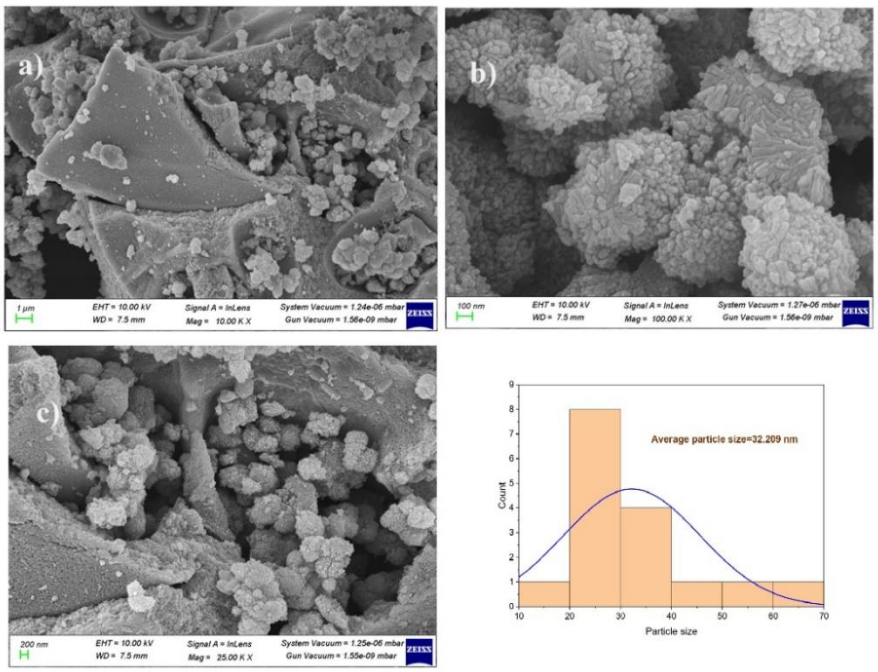

Fig. 4: SEM images of $SrFe_{12}O_{19}/CuO/TiO_2$ (a) 1µm (b)100 nm (c) 200 nm (d) particle size distribution of $SrFe_{12}O_{19}/CuO/TiO_2$ (SEM)

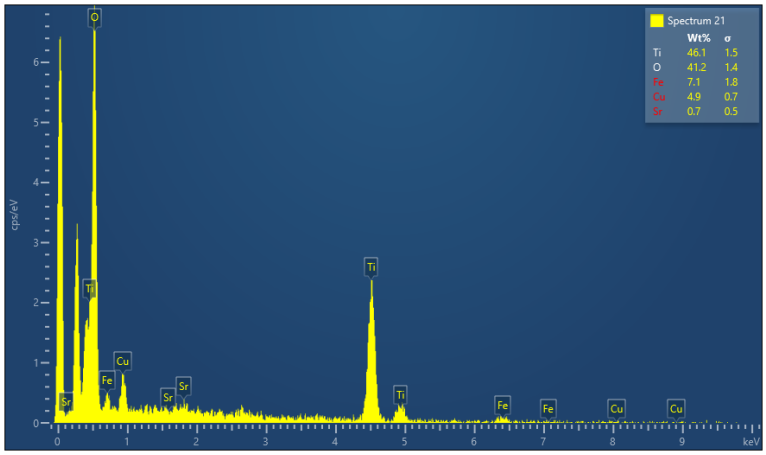

Fig. 5: EDX spectrum of $SrFe_{12}O_{19}/CuO/TiO_2$

Table 2
EDX of $SrFe_{12}O_{19}/CuO/TiO_2$

Element	Wt %	Atomic %
O	41.21	68.68
Ti	46.13	25.68
Fe	7.06	3.37
Cu	4.95	2.08
Sr	0.66	0.20
Total	100.00	100.00

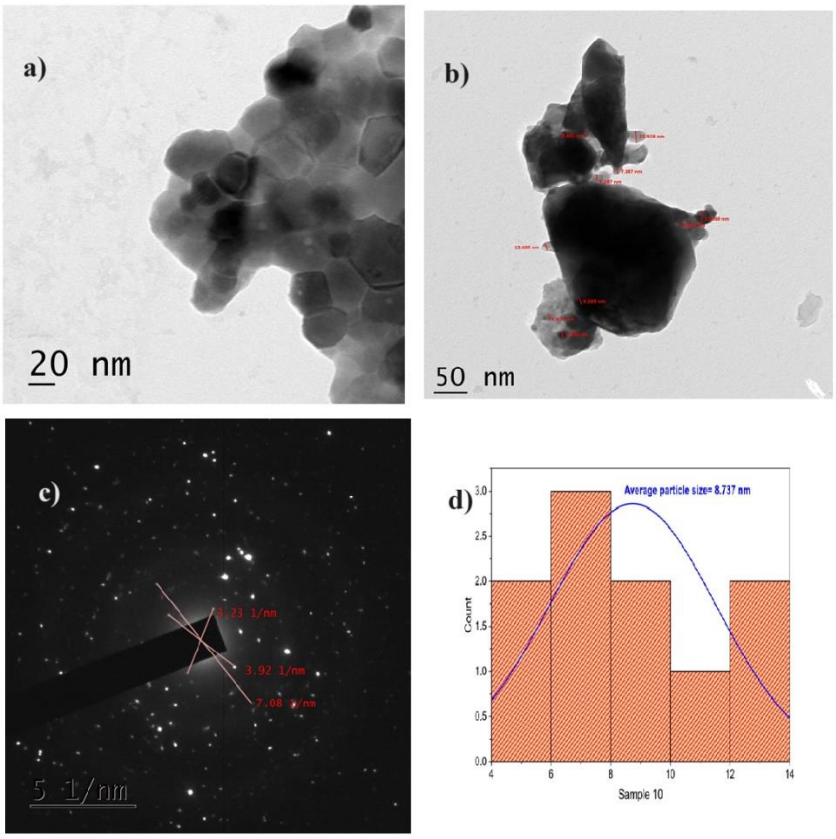

Fig. 6: TEM images of $SrFe_{12}O_{19}/CuO/TiO_2$ (a) 20 nm (b) 50 nm (c) SAED pattern (d) particle size distribution of $SrFe_{12}O_{19}/CuO/TiO_2$(TEM)

TEM studies: Figure 6 shows the typical transmission electron micrographs of the as-prepared $SrFe_{12}O_{19}/CuO/TiO_2$ composite. $SrFe_{12}O_{19}/CuO/TiO_2$ nanostructures agglomerated after coating, as illustrated in fig. 6 a and b, which may be due to magnetic attraction between $SrFe_{12}O_{19}$ particles and the creation of necking zones between the layers covered on the particles. The application of appropriate surfactants will aid in the reduction of agglomeration. The images depict the core/shell/shell structure of the $SrFe_{12}O_{19}/CuO/TiO_2$ composite well, in which the rough surface created by TiO_2 crystals contrasts with the comparatively smooth surfaces made by deposited amorphous CuO. A granular shell comprises of tiny particles ranging in size from 5 to 15 nm (Fig. 6b). The average particle size measured is 8.7 nm (Fig. 6d).

FTIR analysis: Fourier-transform infrared (FTIR) spectroscopy is extremely useful for detecting functional molecule groups because each unique chemical bond absorbs infrared radiation at specific frequencies, resulting in discrete absorption bands. FTIR is an effective instrument for detecting the exact sorts of bonds found in a material. Researchers may collect extensive structural and bonding information about complicated compounds by studying their absorption bands, including insights on binding strength and type. Figure 7 shows the FTIR spectrum of the freshly manufactured $SrFe_{12}O_{19}/CuO/TiO_2$ nanostructures, showing significant aspects of their molecular structure. The bands at 2892 cm^{-1} and 3871 cm^{-1} represent symmetric and asymmetric stretching vibrations of the O-H bond respectively confirming the presence of hydroxyl groups.

The bands at 522 cm^{-1} represent the bending vibration of the Cu-O bond, indicating the presence of copper oxide components in the nanostructure. Additionally, the signal at 1582 cm^{-1} indicates the stretching vibration of the Cu-O bond in copper (II) oxide, indicating the existence of CuO in the composite. The band at 471 cm^{-1} indicates lattice absorption of Fe-O bonds, confirming the integration of $SrFe_{12}O_{19}$ into the nanostructure. The band at 436 cm^{-1} represents the stretching vibrations of Ti-O-Ti bonds at octahedral sites, indicating the presence of titanium oxide in the composite.

Overall, the FTIR spectrum gives thorough proof of the bonds and functional groups in the $SrFe_{12}O_{19}/CuO/TiO_2$ nanostructures, confirming the effective production of the composite material with the desired chemical composition.

Magnetic properties: At room temperature 300K, the magnetic characteristics of the synthesized $SrFe_{12}O_{19}/CuO/TiO_2$ nanocomposite sample were measured using a VSM (Vibrating sample magnetometer). The shape and size of the nanoparticle have a significant impact on the magnetic characteristics of the material. Figure 8 depicts the hysteresis

loop formed as an "S" shape curve, demonstrating the material's soft ferromagnetic behaviour. The hysteresis curve shows that the utterly saturated position was not achieved. The saturation magnetization of $SrFe_{12}O_{19}/CuO/TiO_2$ nanoparticles is measured at 162.72 emu/g, which is much lower than the saturation magnetization of a single $SrFe_{12}O_{19}$ nanostructure.

Photocatalytic studies: The $SrFe_{12}O_{19}/CuO/TiO_2$ nanocomposite is tested for its capacity to destroy methylene blue (MB) dye in an aqueous solution under visible light conditions utilizing various processing techniques. This study assessed the nanocomposite's efficiency and efficacy as a photocatalyst. Before testing the nanocomposite's photocatalytic degradation capabilities, a control experiment was performed in which the MB dye solution is subjected to visible light without adding composite nanoparticles. The blank experiment revealed no substantial degradation of the methylene blue dye, demonstrating that visible light alone was inadequate to break down the dye without a photocatalyst.

Effect of initial dye concentration: The study investigated the influence of different starting concentrations of methylene blue (MB) dye on the photocatalytic degradation process to establish the best concentration for efficient degradation. The initial dye concentrations varied between 5 and 100 ppm, with a constant catalyst dosage of 500 mg. This technique sought to determine the concentration at which deterioration efficiency was maximum.

The findings revealed that the degradation efficiency improved as the dye concentration increased from 5 to 100 ppm. This tendency can be due to the increased amount of dye molecules accessible for interaction with the photocatalyst, which improves the total degradation rate. However, after the dye concentration hits a specific level, the degradation efficiency declined. This decrease in effectiveness at greater dye concentrations was most likely caused by the saturation of active areas on the composite material's surface. With more dye molecules present, there are fewer active sites for the photocatalytic process, resulting in a decrease in degradation efficiency.

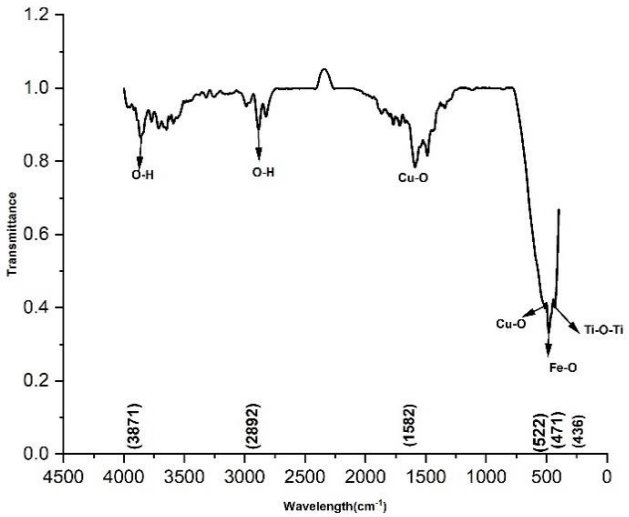

Fig. 7: FTIR of $SrFe_{12}O_{19}/CuO/TiO_2$

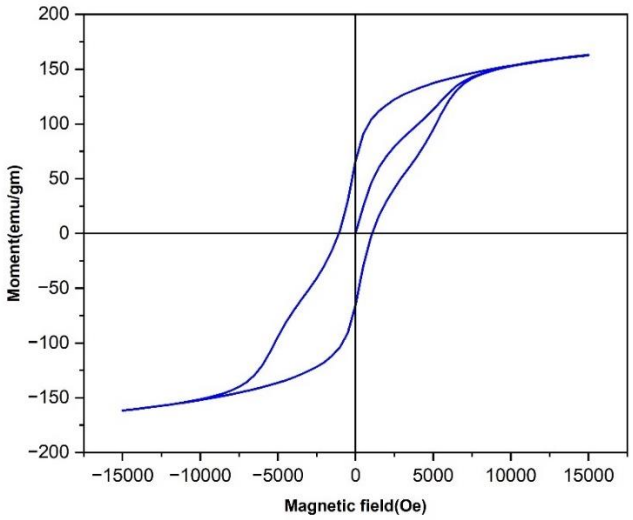

Fig. 8: Magnetization loop for $SrFe_{12}O_{19}/CuO/TiO_2$ composite

Figure 9 shows the connection between the initial concentration of MB dye and its degradation efficiency. The results showed that an initial dye concentration of 10 ppm was best. At this concentration, the photocatalytic activity destroyed the dye after 130 minutes. This data indicates that 10 ppm is the optimal starting concentration for obtaining maximal degradation efficiency with the given catalyst dosage.

Effect of pH of initial dye solution: The pH of the solution is a crucial element in photocatalytic processes because it affects the surface charge of the photocatalyst. Figure 10 depicts the influence of different pH levels (4-8) on the photocatalytic degradation rates of $SrFe_{12}O_{19}/CuO/TiO_2$ materials. The results showed that photocatalytic degradation rates were best at pH 6, 7 and 8. These findings show that the photocatalyst's surface charge under these pH settings is ideal for increasing methylene blue dye breakdown. At these pH values, the photocatalyst's surface charge most likely allows for more effective interactions between the catalyst and the dye molecules, increasing photocatalytic activity.

In acidic conditions (pH < 6), breakdown efficiency reduces. The high concentration of protons in the solution competes with dye molecules for active sites on the photocatalyst's surface, resulting in a loss in efficiency. Excess protons can also generate a positive charge on the photocatalyst's surface, rejecting positively charged dye molecules and delaying their breakdown. The ideal pH range of 6 to 8 resulted in 100% degradation efficiency after 90 minutes.

Effect of temperature: The study looked at the degradation of methylene blue (MB) dye at four distinct temperatures (30 °C, 35 °C, 40 °C and 45 °C) while maintaining all other variables constant. Figure 11 depicts the catalyst's C/C_0 vs. reaction temperature where C_0 represents the starting concentration of methylene blue and C represents the concentration of methylene blue at a certain time. The findings show that raising the reaction temperature improves the photodegradation effectiveness of the MB dye when utilizing the catalyst. At all measured temperatures, the degradation efficiency was 100%, however, the time required for complete deterioration varied. At 30 °C, 35 °C and 40 °C, the photocatalytic degradation of MB dye reached 100% across varying periods. However, the optimal temperature for the deterioration process is discovered to be 45 °C. At this temperature, photocatalytic activity achieved 100% efficiency in 55 minutes, indicating the quickest degradation rate among the investigated temperatures.

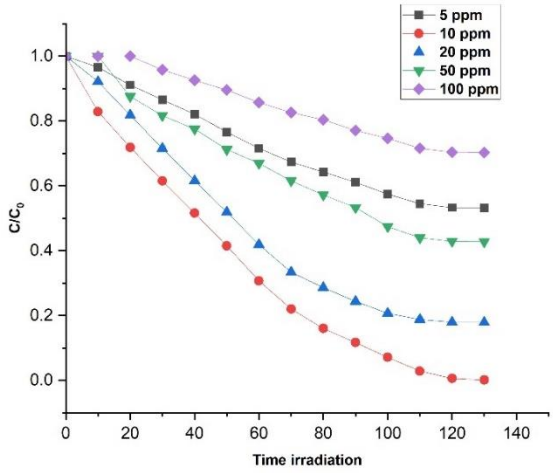

Fig. 9: Effect of initial dye concentration on the photocatalytic degradation of MB dye, Catalyst load = 500mg

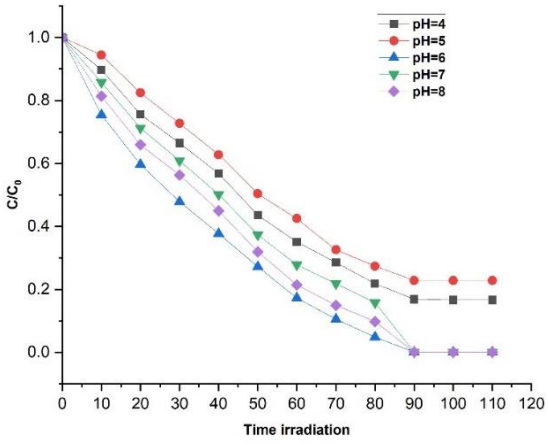

Fig. 10: Effect of pH on initial dye solution; catalyst load = 500mg, [Dye] =10 ppm(fixed)

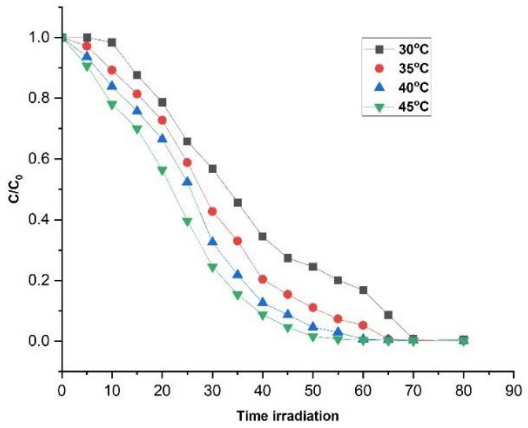

Fig. 11: Effect of temperature on visible light-induced photocatalytic degradation of MB dye; catalyst load = 500 mg, [Dye] = 10 ppm (fixed), pH = 6 (fixed)

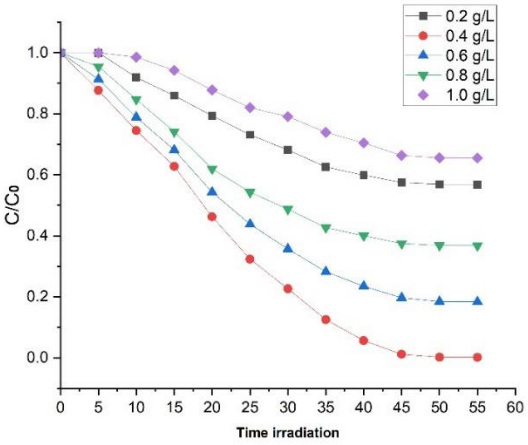

Fig. 12: Effect of catalyst loading on the degradation efficiency of methylene blue under visible light irradiation, catalyst load = 500 mg, [Dye] = 10 ppm (fixed), pH= 6 (fixed), temperature = 45 ºC (fixed)

Effect of catalyst loading: The impact of photocatalyst loading on the photocatalytic degradation of methylene blue dye is investigated using $SrFe_{12}O_{19}/CuO/TiO_2$ nanomaterials. The catalyst dose ranged from 200 mg to 1000 mg per 100 mL of dye solution and all tests were performed at room temperature. Figure 12 explains the connection between catalyst dose and degradation efficiency. The data in the figure show a clear trend. As the catalyst dose grew, so did the methylene blue dye's degradation efficiency. However, it is worth noting that at a catalyst dose of 400 mg, the degradation efficiency reached 100% after 50 minutes. These findings suggest that this dose is enough for complete dye degradation under the testing circumstances.

Effect of irradiation time: Irradiation duration is another crucial element influencing photocatalytic efficiency for methylene blue (MB) dye removal using TiO_2, CuO, $SrFe_{12}O_{19}$ and $SrFe_{12}O_{19}$-CuO-TiO_2 nanocatalysts. The experiment was conducted at a pH of 6 with irradiation periods ranging from 0 to 55 minutes, while all other parameters remained constant. Figure 13 shows the connection between degradation efficiency (C/C0) and irradiation time. The degradation efficiency, which measures how much dye concentration is lowered over time, rose for all photocatalysts when the irradiation period was raised to 50 minutes.

Beyond this time, the deterioration efficiency plateaued, suggesting no more substantial degradation beyond 50 minutes**.** The best irradiation length for all samples was 50 minutes, with dye removal efficiencies of 14.9 %, 55.6 %, 69.9 % and 99.6 % for TiO_2, CuO, $SrFe_{12}O_{19}$ and $SrFe_{12}O_{19}$-CuO-TiO_2 catalysts respectively. These findings show that the $SrFe_{12}O_{19}/CuO/TiO_2$ nanocatalyst had the best photocatalytic efficiency, reaching nearly the destruction (99.6%) of the MB dye within 50 minutes of irradiation. This improved performance is due to the synergistic effects of mixing $SrFe_{12}O_{19}$, CuO and TiO_2 which increase total photocatalytic activity.

Re-usability of catalysts: The re-usability of the $SrFe_{12}O_{19}$/ CuO/TiO_2 composite catalyst was examined under ideal circumstances to determine its suitability for recurrent usage

in photocatalytic degradation processes. Following each reaction cycle, the catalyst was collected and washed adequately with distilled water and ethyl alcohol to eliminate any remaining colour or impurities. To assess re-usability, the composite was recycled three times using methylene blue (MB) concentration profiles to track degradation efficiency across several cycles. The results show that as the catalyst was re-used, the degrading efficiency gradually decreased (Fig. 14). The catalyst was obtained an 84 % removal efficiency in the first run which dropped marginally to 78 % in the second run and 60 % in the third. Despite this decrease, the re-usability of the $SrFe_{12}O_{19}/CuO/TiO_2$ composite is still relatively high, indicating its stability and potential for recurrent usage.

Antibacterial activity: It can be observed that the catalyst has shown good antibacterial activity against all the selected Gram-positive bacteria *Staphylococcus aureus* and *Bacillus subtilis* and Gram-negative bacteria *Escherichia coli*, *Klebsiella pneumonia*. The selected catalyst has displayed good antibacterial activity.

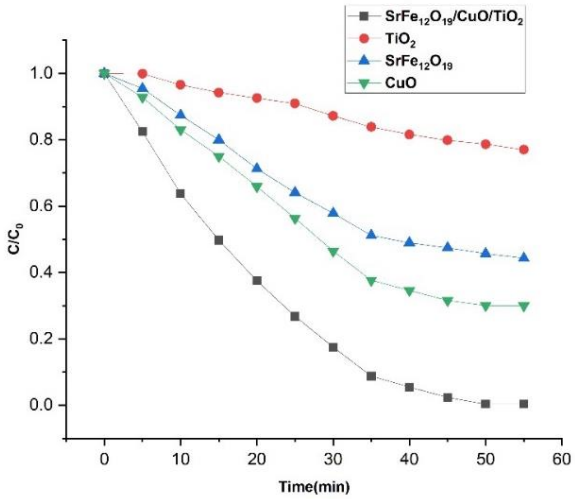

Fig. 13: Plots of C/C_0 of Methylene blue for CuO, TiO_2, $SrFe_{12}O_{19}$ and $SrFe_{12}O_{19}$-CuO-TiO_2 photocatalysts.

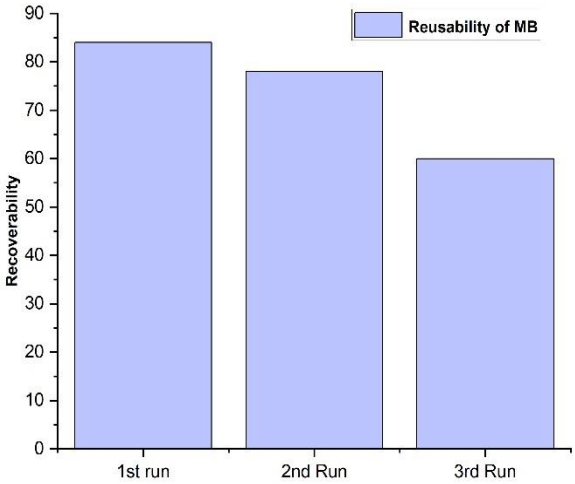

Fig 14: Reusable capacity of $SrFe_{12}O_{19}/CuO/TiO_2$ Nano composite of Methylene blue

Table 3
Antibacterial activity of $SrFe_{12}O_{19}/CuO/TiO_2$

Antibacterial Activity of the Catalysts				
Compounds	**Zones of inhibition (diameter in mm), 0.125 µg/mL**			
	Gram-positive		**Gram-negative**	
	SA	BS	KP	EC
$SrFe_{12}O_{19}/CuO/TiO_2$	20	24	32	29
Ampicillin	28	36	35	37
SA = *Staphylococcus aurues*; BS = *Bacillus subtilis*; KP = *Klebsiella Pneumoniae*; EC = *Escherichia coli*				

Conclusion

Photocatalytic experiments revealed that $SrFe_{12}O_{19}$/ CuO/TiO_2 nanocomposites had a 100% degradation efficiency against methylene blue dye. Under visible and UV irradiation, the synthesized $SrFe_{12}O_{19}/CuO/TiO_2$ sample with a molar ratio of 0.8: 0.1: 0.1 displayed high catalytic efficiency. 400 mg of catalyst for 10 ppm of dye in 100 mL at 45 °C and pH range of 6-8 resulted in 100% degradation of methylene blue dye. The catalyst might be re-used up to three times to effectively degrade the colour.

The antibacterial activity was investigated against Gram-positive *Staphylococcus aureus*, *Bacillus subtilis* bacteria and Gram-negative *Escherichia coli*, *Klebsiella pneumonia*, using nanocomposites and the results are comparable to the standard ampicillin antibacterial drug.

Acknowledgement

The authors thank Advanced Analytical Laboratory, Andhra University, Visakhapatnam, India, for providing the spectral analysis.

References

1. Bruno L., Cíntia Z.F.P., João A.P. and Julio C.P., Effects of textile dyes on health and the environment and bioremediation potential of living organisms, *Biotechnology Research and Innovation*, **3(2)**, 276 **(2019)**

2. Esther F., Tibor C. and Gyula O., Removal of synthetic dyes from wastewaters: a review, *Environment International*, **30**, 953 **(2004)**

3. Grégorio C. and Eric L., Advantages and disadvantages of techniques used for wastewater treatment, *Environmental Chemistry Letters*, **17**, 149 **(2019)**

4. Guidong Y., Zheng J., Huahong S., Tiancun X. and Zifeng Y., Preparation of highly visible-light active N-doped TiO_2 photocatalyst, *Journal of Materials Chemistry*, **20**, 5301 **(2010)**

5. Hafsa S., Mohammad R.P., Qureshi M.S., Malik M.M. and Fozia Z.H., Studies of structural, optical and electrical properties associated with defects in sodium-doped copper oxide (CuO/Na) nanostructures, *Journal of Material Science*, **53**, 8828 **(2018)**

6. Keiichi T., Kanjana P. and Teruaki H., photocatalytic degradation of commercial azo dyes, *Water Research*, **34(1)**, 327 **(2000)**

7. Kheirollah M., Masoud S. and Rohollah A., Facile synthesis of $SrFe_{12}O_{19}$ nanoparticles and its photocatalyst application, *Journal of Materials Science: Materials in Electronics*, **28**, 10043 **(2017)**

8. Paramdeep K., Anupama K. and Sonal S., Comparative evaluation of photocatalytic performance of hexagonal ferrites procured via sol-gel route, Materials Today: Proceedings, **14**, 427 **(2019)**

9. Shakeel K., Awal N., Idrees K. and Niaz M., Photocatalytic Degradation of Organic Dyes Contaminated Aqueous Solution Using Binary $CdTiO_2$ and Ternary $NiCdTiO_2$ Nanocomposites, *Catalysts*, **13(1)**, 1 **(2023)**

10. Shreyasi P., Soumen M., Uday N.M. and Kalyan K.C., Low temperature solution processed ZnO/CuO heterojunction photocatalyst for visible light induced photo-degradation of organic pollutants, *Cryst Eng Comm*., **17**, 1465 **(2015)**

11. Sijing C., Yongjiang D., Hang l., Mengyu W., Bi J., Rong X. and Xiaoyan Liu, Efficient photocatalytic dye degradation by flowerlike $MoS_2/SrFe_{12}O_{19}$ heterojunction under visible light, *Applied Surface Science*, **559**, 2 **(2021)**

12. Somasekhar R. and Paul Douglas S., Graphene oxide–nano-titania composites for efficient photocatalytic degradation of indigo carmine, *Journal of the Chinese Chemical Society*, **65(12)**, 1423 **(2018)**

13. Richa T., Sharma M.K. and Ameta S.C., Improvement in the Quality of Bromophenol Blue Containing Polluted Water after Photocatalytic Treatment, *Oriental Journal of Chemistry*, **27(2)**, 741 **(2011)**

14. Rui W., Jiashun C., Jiajia L. and Yifei Z., Synthesis of $CuO@TiO_2$ nanocomposite and its photocatalytic and electrochemical properties-Application for treatment of azo dyes in industrial wastewater, *International Journal of Electrochemical Science*, **18(12)**, 2 **(2023)**

15. Vinothkumar P., Manoharan C., Shanmugapriya B. and Mohammed B., Effect of reaction time on structural, morphological, optical and photocatalytic properties of copper oxide (CuO) nanostructures, *Journal of Materials Science: Materials in Electronics*, **30**, 6249 **(2019)**

16. Wenjuan L., Robert L., Anming H., Zhaohui H. and Norman Z.Y., Generation of oxygen vacancies in visible light activated one-dimensional iodine TiO_2 photocatalysts, *RSC Advances*, **4**, 36960 **(2014)**

17. Yumatorn M., Dang T.T.T., Duangdao C., Wilawan K. and Auppatham N., Decomposition of dye pigment via photocatalysis process using $CuO\text{-}TiO_2$ nanocomposite, Materials Today: Proceedings, **47**, 3441 **(2021)**.

(Received 17th September 2024, accepted 20th November 2024)